Short Papers

Achieving Versatile Energy Efficiency With the WANDERER Biped Robot

Clinton G. Hobart, Anirban Mazumdar, Steven J. Spencer, Morgan Quigley, Jesper P. Smith, Sylvain Bertrand, Jerry Pratt, Michael Kuehl, and Stephen P. Buerger

***Abstract*—Legged humanoid robots promise revolutionary mobility and effectiveness in environments built for humans. However, inefficient use of energy significantly limits their practical adoption. The humanoid biped walking anthropomorphic novelly-driven efficient robot for emergency response (WANDERER) achieves versatile, efficient mobility, and high endurance via novel drive-trains and passive joint mechanisms. Results of a test in which WANDERER walked for more than 4 h and covered 2.8 km on a treadmill, are presented. Results of laboratory experiments showing even more efficient walking are also presented and analyzed in this article. WANDERER's energetic performance and endurance are believed to exceed the prior literature in human-scale humanoid robots. This article describes WANDERER, the analytical methods and innovations that enable its design, and system-level energy efficiency results.**

***Index Terms*—Energy efficiency, humanoid robots, legged locomotion, torque control.**

I. Introduction

Legged robots offer tremendous potential for mobility, but their practical use to date has been minimal, in part due to inefficient use of energy. The legged robots that can operate and conduct meaningful physical work at a scale similar to humans are expected to be particularly useful for traversing and working in the built-for-humans world, e.g., in support of manufacturing, medical, or emergency response activities. To be practical in such applications, robots must be able to conduct a wide variety of different mobility and manipulation tasks, and also carry their own energy supply, without tethers while locomoting for hours, potentially over multi-km distances. Extremely energy-efficient walkers have been demonstrated, e.g., by sculpting the robots' passive dynamics optimally for walking at a single speed on level ground. However, these platforms are fundamentally limited to small sets of tailored behaviors [1]. Conversely, highly capable robotic platforms have been developed, e.g., using hydraulics to achieve high power density and a variety of impressive physical feats [2]. However, the powertrain for these platforms is extremely inefficient, with input power for robots at adult human scale running well into the multi-kW range [2]. Many electrically-powered legged platforms exist with various levels of capability and power (e.g., [3]–[7]). Some research platforms only achieve planar walking and require external support to balance [3]. Others approach the full range of human motion capability at approximately human scale [4]–[7]. In general, none of these overcome the fundamental tradeoff between functionality and efficiency in legged platforms.

Recent works have addressed energy efficiency in legged platforms. The MIT Cheetah achieved high running speeds and also efficient mobility [8], [9]. It uses large motors with modest gearing, but is designed primarily for a high-speed, high-frequency regime. ATRIAS achieves high-efficiency spring-mass walking, and exploits resonance for efficiency under particular gait conditions [10]. DURUS uses low friction, high gear ratio cycloidal transmissions to walk efficiently [11]. In contrast, our work focuses on efficient operations across a wide variety of bipedal behaviors. Unlike other bipeds, our robot utilizes minimal gear reductions and is fully backdrivable without torque feedback. Few, if any, results have been reported in the literature describing the performance of such designs when walking over long distances or with a variety of gaits.

In this article, we describe the humanoid biped walking anthropomorphic novelly-driven efficient robot for emergency response (WANDERER), an all-electric robot that achieves energy efficiency across a variety of locomotive behaviors. WANDERER is human-scale (2.0 m tall, 91 kg mass), fully self-contained, has 29 degrees-of-freedom (DOF) and a projected range of nearly 4 km. To achieve high endurance, apparently unmatched by versatile, human-scale humanoid robots in the literature to date, WANDERER's development adhered to three main principles: first, the actuator size is optimized in order to minimize Joule (I^2R) heating losses, second, a core drivetrain provides high-quality torque control with minimal gearing and without torque feedback, limiting losses almost exclusively to I^2R heating in the motors [12], [13], and third, passive joint-level mechanisms are optimized to limit the peak torques that dominate I^2R losses. WANDERER's design may seem counter-intuitive: the motors are as large as can be practically packaged; the lower body is fully backdrivable with no passive postural support, and entirely limp when unpowered.

Manuscript received June 28, 2019; accepted December 20, 2019. Date of publication February 21, 2020; date of current version June 4, 2020. This paper was recommended for publication by Associate Editor P. M. Wensing and Editor E. Yoshida upon evaluation of the reviewers' comments. This work was supported by the Defense Advanced Research Projects Administration as part of the Maximum Mobility and Manipulation Program. Sandia National Laboratories is a multimission laboratory managed and operated by National Technology and Engineering Solutions of Sandia, LLC, a wholly owned subsidiary of Honeywell International Inc., for the U.S. Department of Energy's National Nuclear Security Administration under Contract DE-NA0003525. *(Corresponding author: Stephen P. Buerger.)*

C. G. Hobart, S. J. Spencer, M. Kuehl, and S. P. Buerger are with Sandia National Laboratories, Albuquerque, NM 87185 USA (e-mail: cghobar@sandia.gov; stespenc0383@gmail.com; mkuehl@sandia.gov; sbuerge@sandia.gov).

A. Mazumdar was with Sandia National Laboratories, Albuquerque, NM 87185 USA. He is now with the Department of Mechanical Engineering, Georgia Institute of Technology, Atlanta, GA 30332 USA (e-mail: anirban.mazumdar@me.gatech.edu).

M. Quigley is with the Open Source Robotics Foundation, Mountain View, CA 94041 USA (e-mail: morgan@openrobotics.org).

J. P. Smith was with the Florida Institute for Human and Machine Cognition, Pensacola, FL 32502 USA. He is now with Halodi Robotics, 1599 Moss, Norway (e-mail: mail@jespersmith.nl).

S. Bertrand and J. Pratt are with the Florida Institute for Human and Machine Cognition, Pensacola, FL 32502 USA (e-mail: sbertrand@ihmc.us; jpratt@ihmc.us).

This article has supplementary downloadable material available at https://ieeexplore.ieee.org, provided by the authors.

Color versions of one or more of the figures in this article are available online at http://ieeexplore.ieee.org.

Digital Object Identifier 10.1109/TRO.2020.2969017

IEEE Transactions on Robotics (T-RO) paper, presented at IROS 2020. It should be cited as a T-RO paper.

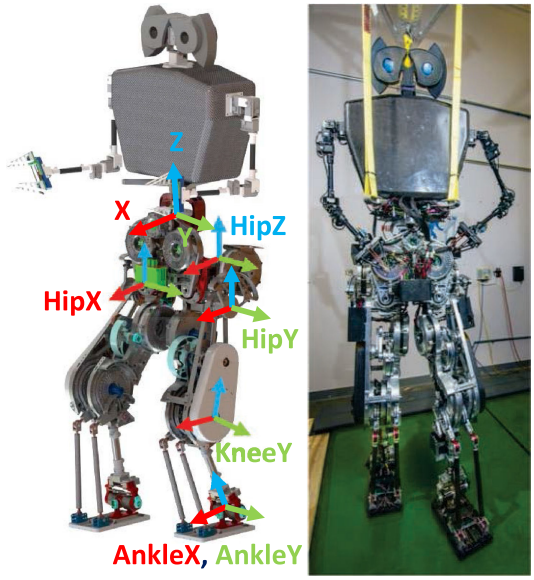

Fig. 1. Rendering (left) and photo (right) of WANDERER.

The contributions of this article are the sizing analysis for the core actuators and drivetrain, and the experimental evaluation over long time-scales and across a range of behaviors. The value of these contributions is illustrated by the performance of WANDERER when compared to its testbed predecessor known as STEPPR [14]. The analysis methods and design improvements outlined in this work enabled WANDERER to use less than half the energy of STEPPR, consume low power over a variety of gaits, and perform far more reliably.

This article begins with a description of how design principles for energy efficient locomotion were extended and integrated to enable WANDERER's improved performance and efficient locomotion. Section III presents results of endurance testing for level ground walking and other locomotive behaviors. Section IV concludes this article.

II. Enabling Energy-Efficient Locomotion

This section describes how advances in energy efficient features for humanoid bipeds, some of which have been described in our prior works, have been developed for use in a new versatile robot that achieves more than a 50% reduction in energy consumption versus its predecessor.

A. Robot Configuration

WANDERER's motion is described with a body fixed coordinate system centered at its center of mass (see Fig. 1). The X axis points forward, the Y axis to the robot's left, and the Z axis upwards. Leg joint angles are measured relative to the proximal link in the kinematic chain. Each leg has six actively-controlled joints: three at the hip, one at the knee, and two at the ankle. Joints are arranged serially, except for the ankle joints that are driven differentially by motors located in the robot's knees via pushrods. The order of the hip joints, from proximal to distal, is: X (abduction/adduction), Z (internal/external rotation), Y (flexion/extension). The leg axes are labeled in Fig. 1. Three serial harmonic-drive joints move the torso relative to the pelvis. The torso contains batteries and control computers. Two light-duty 6-DOF arms and a 2-DOF neck do not significantly affect locomotive efficiency. Improvements from STEPPR include larger motors for some axes, and optimized new designs for fully integrated passive joint mechanisms that were previously treated as add-ons [14]. These changes are discussed in the following.

B. Low-Loss Joint Drivetrain

WANDERER's core drivetrain (its motors and cable transmissions) limits energy loss by: first, reducing friction losses to insignificant levels, second, limiting gear ratios to avoid expending energy to overcome reflected inertia and friction, and third, scaling motors to minimize I^2R losses. The transmissions described in [13] virtually eliminate joint friction and satisfy packaging constraints by using synthetic polymer (lubricated, braided Vectran) cables in a continuous-bend-on-sheave configuration to achieve 94% efficiency across typical joint trajectories. While cable elasticity can be a challenge and places limits on performance [15], our measured torque output bandwidth was 28 Hz, which is suitable for legged locomotion. This high bandwidth combined with low friction enables effective torque tracking by current control, without the need to modify the intrinsic dynamics with torque feedback [12].

Implementing flexible walking that can tolerate slight position measurement errors and unmodeled terrain variations requires low mechanical output impedance (low apparent inertia and friction) in the drivetrain. The low gear ratios at WANDERER's joints eliminate any need for torque feedback to reduce apparent inertia and friction. This is crucial to the robot's energetic performance because using torque feedback to reduce undesired dynamics requires power from the drive motors [16]. This power can be quite significant, even if the drivetrain does zero output work. This is illustrated in detail in [12] with an analysis focused on calculating loss in electric motors for a range of relevant conditions. Methods are not yet developed to quantify or optimize drive system impedance that is "low enough" for quality torque control. As a rule of thumb, we targeted gear ratios of 10:1 or less, resulting in reflected joint actuator moments of inertia at least $2\times$ smaller, and in most cases $\sim 10\times$ smaller than those of the corresponding robot links throughout WANDERER's legs. Reflected actuator friction is similarly minimized. The drivetrain efficiency was further improved relative to STEPPR by incorporating more thermally efficient motor housings with active cooling as detailed in [17].

C. Motor Scaling

With these modest joint gear ratios, relatively large, high-torque motors are needed to achieve joint-level requirements. The role of motor size is briefly discussed in [12], and key motor parameters and drivetrain parameters were examined in [11], [18], and [19]. However, these previous works have not addressed motor scaling on multijoint robot systems. The analysis below provides a methodology to guide motor selection for particular kinematics, and is a core contribution of this work. This analysis, which assumes fixed mass distribution, was used to design WANDERER and improve its performance.

The use of small motors reduces overall robot size and mass, thereby reducing required joint torques. However, the motor constant K_m increases with motor size and mass, meaning that larger motors dissipate less energy per unit torque. Understanding the tradeoff between these effects is critical to optimizing motor size for efficiency. Building on the analysis in [12], the total electrical energy supplied to a single motor while walking may be expressed in terms of the joint torque and velocity τ and ω, respectively, as

$$E_M = \int \frac{\tau^2}{N^2 K_m^2} dt + \int \tau \omega dt \tag{1}$$

where N is the gear ratio of the transmission, and the time integrals span a fixed number of gait cycles. The first term describes I^2R heating in the windings, and the second describes mechanical output work. When walking on flat ground, the only net mechanical work is from frictional energy dissipation in the joints, drivetrain and ground interaction. In low-friction legged systems, I^2R losses are a large fraction of the total electrical energy. For example, 76% of the MIT Cheetah's [8] and ∼95% of Sandia's STEPPR's motor input power was so consumed.

In designing WANDERER, we considered modest changes to motor selection from the STEPPR design, focusing on joints that consume substantial energy when walking and considering only alternatives that could be feasibly packaged. Because changing motor mass affects torque at all joints, motor scaling is considered at a system level. The average I^2R losses at an individual motor are denoted by $p_{J,i}$, where τ_i is the root mean squared torque, N_i is the gear reduction ratio, and $K_{m,i}$ is the motor constant, all at the ith joint as

$$p_{J,i} = \frac{\tau_i^2}{N_i^2 K_{m,i}^2}. \tag{2}$$

For the family of motors (AlliedMotion Megaflux) used in STEPPR and WANDERER, K_m scales ∼linearly with the motor mass, m_m. The continuous and peak torque scale similarly with mass. So, as motor options are compared, the following expression is used, with $\beta = 0.5$ derived from motor datasheets:

$$K_{m,i} \approx \beta m_{m,i}. \tag{3}$$

Since the joints primarily accelerate the robot or support it against gravity, we assume that the joint torques are roughly proportional to the robot mass, $m_R : \tau_i \propto m_R$. Therefore

$$p_{J,i} \propto \frac{m_R^2}{N_i^2 \beta^2 m_{m,i}^2}. \tag{4}$$

For the second term in (1), the frictional losses at the ith joint are denoted $p_{f,i}$, the product of joint torque from friction $\tau_{f,i}$ and the joint speed ω_i as

$$p_{f,i} \sim \tau_{f,i}\left(\tau_i, \omega_i\right)\omega_i. \tag{5}$$

Friction torque can depend on load (Coulomb friction) and on speed (viscous/aerodynamic losses). Since this analysis is trajectory-independent, ω_i is invariant with motor selection. Torque τ_i, however, does vary with motor selection. Again, applying the proportionality of torque to mass produces

$$p_{f,i} \propto m_R \omega_i. \tag{6}$$

Thus, increasing robot mass proportionally increases the power to overcome internal friction. To determine changes in the energy consumption with motor scale relative to a baseline design requires only these proportionality relationships—not calculation of actual power. The same analysis may be applied to new systems, working from any baseline analysis or simulations used in the design process for motor sizing.

To evaluate the system-level energy implications of motor size, it is further necessary to estimate how m_R scales with changes to total motor mass, $m_m = \sum_{i=1}^{n} m_{m,i}$. m_R consists of two components: m_m, and the mass of everything else (including the structural frame, computers, batteries, etc.), denoted m_f. A key question is how nonmotor mass, m_f, scales when the total motor mass, m_m, is increased. This depends on robot design details and is difficult to generalize. However, the range of possibilities may be explored as variants from a nominal design. Variants are described by scaling m_m by the factor c_1 and m_f by the factor c_2 as follows:

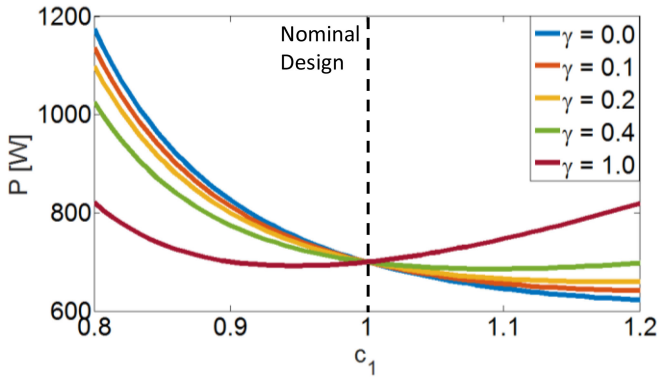

Fig. 2. Computed estimates for motor power for varying degrees of motor mass penalty (γ), and for both added ($c_1 > 1$) and subtracted ($c_1 < 1$) motor mass (8)–(10). The dashed line represents a nominal robot design based on STEPPR.

$$m_{R,0} = m_{m,0} + m_{f,0} \tag{7}$$

$$m_R \sim c_1 m_{m,0} + c_2 m_{f,0} \tag{8}$$

$$\gamma = \frac{c_2 - 1}{c_1 - 1} \tag{9}$$

$$m_R \sim c_1 m_{m,0} + \left(\gamma\left(c_1 - 1\right) + 1\right) m_{f,0}. \tag{10}$$

Equation (7) describes an initial robot configuration, and (8) is a scaled configuration. c_1 or c_2 greater than 1 means that the motor or frame mass increase, respectively. The γ parameter relates c_1 to c_2. At one extreme, if $\gamma = 0$, then changes to the motor mass m_m have no effect on the mass of the rest of the robot, m_f. At the other extreme, if $\gamma = 1$, the frame/extra mass scales in proportion to the motor mass.

The relationship between γ, motor scale, and energy is illustrated with a case study based on deviations from the STEPPR robot. The nominal design uses 700 W total motor power (90% electrical dissipation, 10% mechanical), with $m_m = 15\,\text{kg}$ and $m_f = 65\,\text{kg}$ ($m_R = 80\,\text{kg}$). The knee and hip Y joints use the same motor (1.6 kg) and account for 19% and 16% of the total power, respectively. We study the energetic impact of changing the mass of these two motors for different values of γ, by examining how small changes [increases ($c_1 > 1$) and decreases ($c_1 < 1$)] in motor mass affect projected power. The power consumption at every leg joint, estimated based on (1)–(6), is summed and plotted for a range of γ values in Fig. 2. The shape of the curves reflects the relative sensitivity of robot frame mass to motor mass (γ) for a particular robot design. For small γ, increasing motor size can *save substantial energy*, to a point. For large γ, adding motor mass increases power consumption. In other words, if a robot's mass is particularly sensitive to motor mass, smaller motors are more efficient.

In STEPPR and WANDERER, motor mass is ∼20–25% of the overall mass. When motors are scaled up, the impact on m_f is relatively modest; for these designs $\gamma < 0.1$ is readily achievable. This means that a 10% (1.5 kg) increase in motor mass requires less than a 1% increase in frame mass (0.65 kg). Therefore, based on this analysis, the four hip/knee flexion motors were scaled up by 22% for WANDERER. The projected savings in total motor power is roughly 12% under the assumptions of $c_1 = 1.22$ and $\gamma = 0.1$. In practice, design improvements enabled the nonmotor mass of WANDERER's legs to be less than STEPPR's. This confirms that small γ's are indeed achievable.

D. Support Elements

The characteristics of our drivetrain enable the efficient use of another major energy-saving feature: passive mechanical devices called "support elements (SEs)." SEs are tailored to certain key joints to make the extraction of energy from the motors more efficient. SEs alter the relationship between the instantaneous torque/velocity at the joint and the output of the cable transmissions. They do not (ideally) impact the joint torque or velocity, and therefore do not affect gait. Because they are energy-neutral, they cannot reduce the net mechanical energy required by the joint motors to support locomotion. However, they can extract that energy in a manner that reduces I^2R losses. Conceptually, this is done primarily by limiting peak torques. The SEs described in this article differ substantially from those previously explored.

A data-driven optimization technique was used to identify SE designs that could provide significant energetic benefit across nine representative gaits including human biomechanical data [20], simulated robot data, and experimental robot data for a variety of bipedal behaviors. This analysis identified three unique SEs that saved considerable energy across a variety of gaits: first, selectively engaging springs placed in parallel with the hip ab/adduction (X) motors, second, a selectively engaging spring placed in parallel with the ankle flexion (Y) joint, and third, a four-bar mechanism that provides pose dependent gearing at the knee joints. These SEs are predicted to reduce dissipated power by 38–72%, depending on the gait. Analysis and optimization specifics are in [21]. While previous studies by other groups have examined parallel springs on bipedal robots and demonstrated benefit [3], they have not examined hip X, which can benefit immensely from parallel springs.

Our previous experimental studies have shown how add-on SEs can save considerable energy [14]. This current work provides new results showing how further energetic benefits can be achieved with mechanisms designed into the robot frame, enabling them to be smaller, lighter, and stiffer. WANDERER includes integrated SEs, saving much more energy than previously published results. These mechanisms are shown in Fig. 3 and the accompanying video.

At hip X, compression springs are used to achieve a stiffness of 800 Nm/rad. Each spring is unidirectional, and only active over a portion of the joint's motion, so that it engages during stance and disengages during the swing phase of walking. The WANDERER design, highlighted in the video, utilizes a compression spring with rolling contact. Such a design has not previously been explored for bipedal robot hip motions. At ankle Y, two flat wound torsion springs are used in parallel at each joint to achieve a total stiffness of 400 Nm/rad. The ankle springs are also unidirectional, only engaging during flexion.

The knee joint uses a four-bar mechanism placed in series between the output of the joint's rope transmission and the input of a belt drive to the knee joint. Unlike previous iterations, this compact design is contained within the leg and does not risk collisions between the legs. The belt drive allows the motor to be shifted up in the thigh toward the hip. The four-bar mechanism provides a transmission ratio that varies between 0.6 and 2.8 with joint angle. This mechanism exploits the fact that in many gaits the high-torque and high-speed portions of the trajectory occur at different angles, enabling energy savings through pose-dependent gearing. Details of our design optimization method for support elements, and the physical rationale for each joint mechanism may be found in [21].

These new support elements also helped reduce the hip spacing of WANDERER. The spacing between the left and right legs was reduced from 10.5" to 9," and the lack of protruding features enabled narrower foot placement. This reduced typical peak-to-peak walking motion of the hip X joints from 0.4 to 0.2 rad, causing the peak torques and electrical power (in the absence of support springs described above) at these joints to decrease, respectively, from 180 to 130 Nm and from 300 to 160 W.

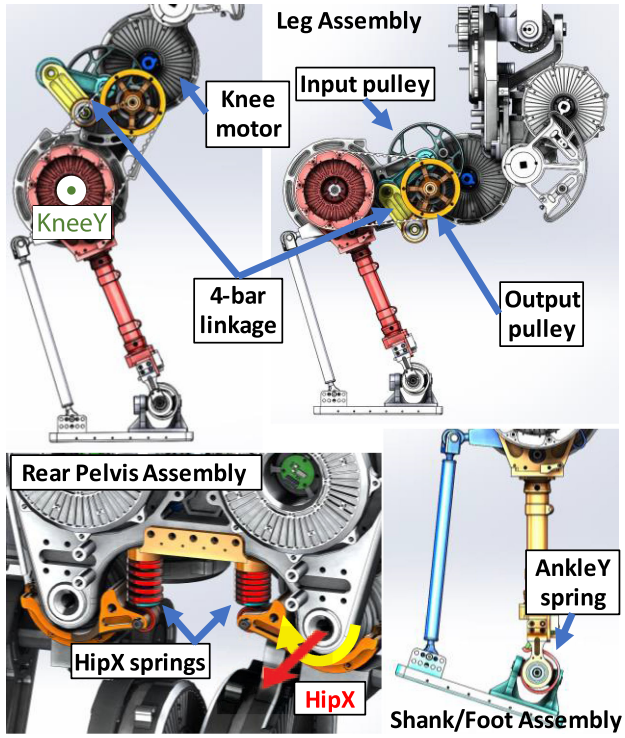

Fig. 3. WANDERER's support elements for knee (top), hip, and ankle (bot).

Our design analysis predicted additional energy reduction from SEs by averaging across all design gaits. The predicted savings are 48% at ankle Y, 61% at knees, 57% at hip X, and a total locomotive power reduction of 49%.

E. Electronics

WANDERER's central control computer calculates torque targets that are realized by a network of controllers located near their respective joints. Joint controllers are arranged in chains (left leg, right leg, torso) using field-programmable gate array (FPGA's) to implement "upstream" and "downstream" 100-MBit Ethernet interfaces. UDP/IP packet parsing and creation is implemented in FPGA logic to increase performance. Microcontrollers throughout the robot continually send sensor data to the nearest joint controller for local use and upstream routing over the Ethernet links.

Energy-conscious actuator design led to 100 V motors, requiring isolated gate drives and analog-digital converters implemented via sigma-delta modulation. Furthermore, because WANDERER uses very little gear reduction, the rotors must be capable of smooth low-speed operation with frequent direction reversals. This is addressed with sensored field-oriented control. A cluster of "sensor microcontrollers" near each joint controller provides on-axis encoding of motor angles, joint angles, temperatures, and other sensors. Each joint controller FPGA and its nearby sensor microcontrollers are connected via USB, allowing the replacement of many delicate sensor wires with a few robust low-cost USB cables. Each USB link is driven by a root host implemented in custom FPGA logic to guarantee 10 kHz real-time communications with the microcontroller's on-chip USB transceiver. The sensors can be tested using standard computers, and then simply plugged into an FPGA-based root host for hard real-time performance.

TABLE I
WANDERER POWER CONSUMPTION

Overhead elements measured separately	Watts
Computers	115.6
Joint controllers – logic (@ 15 joints)	2.7
Arm & neck servos	1.1
Total non-locomotive overhead	*119.4*
Overhead elements measured during walking	
Joint controllers – power overhead (@ 15 joints)	16.7
Zero torque FET switching (@ 15 joints)	33.0
Total locomotive system overhead	*49.7*
Components Measured During Laboratory Walking (Section III-B)	
Computers	111
Knee Y	50
Hip Y	56
Hip X	21
Hip Z	23
Ankles	148
Torso	11
Total Robot Power During Lab Walking	*420*

Motor-level field-oriented control is computed via a custom instruction sequencer in each FPGA to guarantee deterministic computation time in synchrony with the pulsewidth modulation (PWM) pulse train feeding the power stage. The resulting system achieves nearly silent (10 dBA quieter than normal conversation [13]) motor operation at very low, rapidly-changing motor speeds while tracking target currents with >10 Hz variations.

WANDERER is powered by a pair of AllCell HE4820 lithium ion (Li-ion) battery packs with a combined nominal capacity of 2462 Wh and a combined mass of 11.8 kg, mounted in the robot's torso. Table I lists the average power distribution among the various "overhead" components. Losses are divided into those that may be independently measured, and those that are part of the torque production system. Overhead losses are nearly constant across behaviors and are dominated by the ∼116 W consumed by the control and network router computers, which is more than 25% of total robot power during efficient walking. The power consumed by these computers could be reduced by replacing them with custom, power-efficient (e.g., FPGA) implementations. Replacing the router alone could extend walking range by ∼10%. The 15 joint controllers consume ∼17 W when quiescent, and ∼50 W when driving zero current.

F. Walking Control and Sensing

A momentum-based control framework developed by the Florida Institute for Human and Machine Cognition is used to control WANDERER. It uses a quadratic program to solve for given motions in joint-space and tasks-space and ground reaction forces [22]. The control strategy to maintain the robot balance is based on a capture point planning and feedback control framework [23]. This approach allows direct control over the walking speed via user-defined step timing and location while being capable of handling uneven terrain [24]. While the gait generation does not explicitly optimize for energy efficiency, an iterative gait design approach was used to achieve practical blends of robustness and energy efficiency. Candidate gaits were evaluated rapidly via simulations.

In addition to joint position measurements and torque estimates from currents, an inertial measurement unit (Xsens MTI-300) is mounted in the pelvis. Instantaneous pose is estimated by fusing joint angles, torques, and IMU output at 1 kHz. The walking control algorithm provides joint torque updates at 250 Hz, and runs on a small embedded control PC. Ground contact sensors consist of micro-electromechanical systems (MEMS) pressure sensors encapsulated in silicone rubber per the technique by Chuah and Kim [25]. The heel of each foot includes an array of four sensors. Ground contact is detected when the total force exceeds ∼90 N.

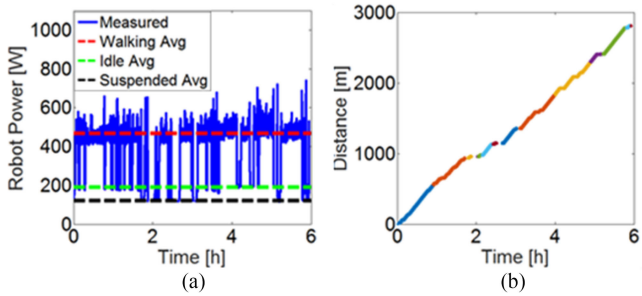

Fig. 4. Time series plots showing power consumption and distance traveled during the 6 h of the DRC endurance walking trial. (a) Plots show the average robot power. (b) The total distance traveled.

TABLE II
FULL BATTERY EXPERIMENTAL ENDURANCE RESULTS

Overall average power	394W
Average power when walking	478W
Average forward walking velocity	0.19 m/s
Powered on time	5:38
Walking / stepping time	4:08

III. ENDURANCE RESULTS

WANDERER was designed to walk long distances over long periods of time, with all batteries and processing carried onboard. Three experiments were designed to evaluate WANDERER's endurance, energetic performance, and gait versatility. These experiments are described in detail in the following.

A. Full-Battery Results

The first experiment was conducted in public at the DARPA Robotics Challenge Finals Technology Exposition (DRC) in Pomona, CA in June, 2015. The experiment was conducted on a treadmill with partial polycarbonate shielding in an outdoor tent. The robot batteries were fully charged and level-ground walking was performed until the battery voltage dropped below the minimum level. The same treadmill was used as in laboratory testing, but the ambient temperature varied by approximately 10 °C and dusty winds of 10–15 mph were typical. An operator controlled the robot walking speed, steering, and treadmill speed with a joystick. This test exposed variability in walking performance, supply voltage, operator fatigue, activities, and ambient conditions.

Summary plots of power and distance traveled are shown in Fig. 4. The robot operated for a total of 5 h 38 m. Over this period, WANDERER walked for 4 h 8 m, and traveled 2.81 km.

In total, 2.23 kWh was extracted from the battery pack, (91% of the nominal capacity). Endurance performance is summarized in Table II. WANDERER walked steadily at an average speed of 0.19 m/s, consuming 478 W (∼370 W locomotive) average power during walking.

The changes in color in Fig. 4(b) indicate restarts of data logging software. In some cases, this was done simply to prevent the data

log file from exceeding a maximum size; in other cases, this was due to WANDERER falling, requiring controller restarts. In total, WANDERER fell nine times. Falls were caused by two known issues: ground contact sensor failures and onboard communication dropouts to one of the legs.

Several elements of the live, sustained experiment led to slightly degraded performance. These include recovery from falls, manual steering to maintain heading, voltage drops due to battery drain, and pauses to mitigate local joint heating. As a result, average power consumption during walking was ∼14% higher than under controlled laboratory conditions, and walking duration was interrupted by occasional falls.

B. Laboratory Walking Detailed Power Analysis

1) Energetic Performance: To analyze WANDERER's power usage and distribution in greater detail, free of the variations present in the prior test, one representative minute of consistent walking was selected from a 42-minute continuous level treadmill walking trial in our laboratory. This period, which provides a manageable volume of data for detailed analysis, includes 50 steps (25 gait cycles) taken after several minutes of continuous walking, ensuring that initial transients had settled. The one minute of data described here is representative of the full 42 min trial. During the one minute period, the robot consumed 420 W average electrical power while walking at an average speed of 0.20 m/s. (The average power over all 42 min was 426 W.) The lab walking is highlighted in the accompanying video, which also illustrates the minimal acoustic emissions from the robot (PWM switching and footfalls dominate the sounds).

The power breakdown is highlighted in Table I. Computing represents 26% of the total power, more than any joint other than the ankles. These results show WANDERER's potential to exceed the performance demonstrated at the DRC. If this power and speed are projected to a full-battery run, then WANDERER would walk for 5.3 h and traverse 3.8 km on a charge (2.23 kWh). These idealized projections reveal the challenges of an extended, remote test: approximately 1 km or 26% of the projected distance was lost due to the issues described in Section III-A. Note that the computing power during walking (111 W) differs slightly from the separate measurement (115.6 W). This small discrepancy likely stems from measurement noise and from variations in battery voltage at the time of measurement.

A common metric for locomotive efficiency is the "actuator cost of transport" (COT), computed from motor power [11]. This lab test shows an actuator-only COT of 1.73 (the full system COT, with computer, is 2.35). While COT is normalized by mass, it does not fully account for endurance considerations. Our COT indicates that roughly 40 W of power is used to carry the battery mass at 0.2 m/s. Reducing battery mass would likely proportionally reduce this cost. This would improve COT, but would also reduce system endurance and practical utility.

2) Support Element Performance: A key factor enabling WANDERER's endurance is the SEs, which were designed based on simulated data and insights gleaned from testing on the STEPPR platform. WANDERER is substantially different in geometry, mass distribution, and walking gait from any of the datasets used to design the SEs. Despite these differences, the three SEs provided substantial energy savings. Since the SEs were designed to be integral to the robot, it is not possible to test the robot without them. Therefore, we evaluate energy savings by comparing measured robot data ("compensated") with model predictions for the power consumption *in the absence of SEs* ("uncompensated"), at each joint. A simple model is used to predict average uncompensated power at joint i, $P_{UC,i}$, based on the root mean square (rms) desired joint torque, $\tau_{d,i}$, commanded by the walking controller as

$$P_{UC,i} = \frac{\tau_{d,i}^2}{K_{m,i}^2 N_i^2}. \tag{11}$$

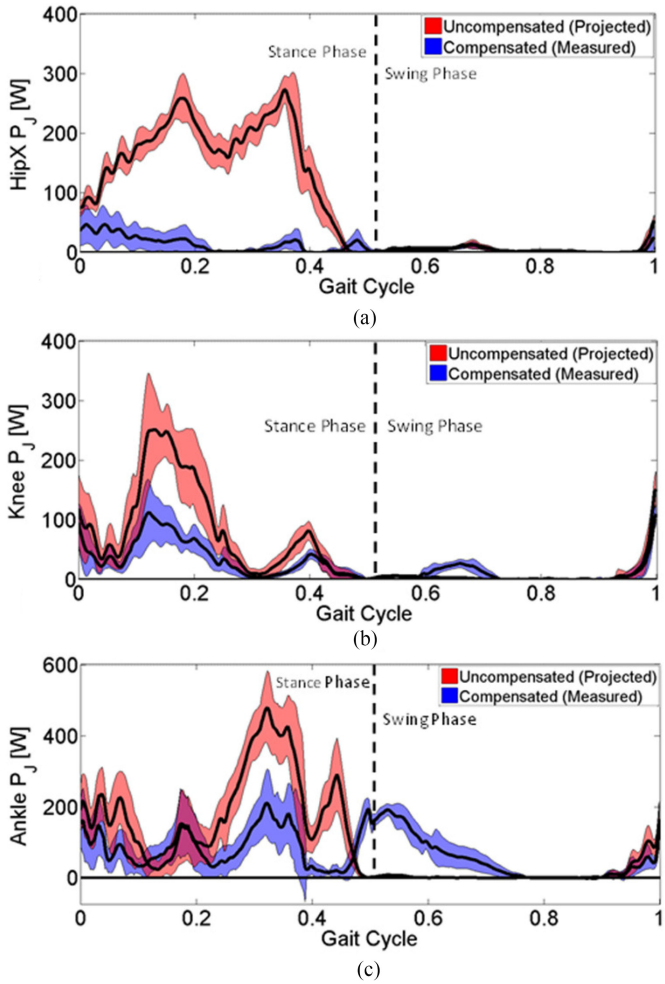

Fig. 5. (a) Hip *X*, (b) knee, and (c) ankle motor power consumption (mean ± standard deviation) for a single leg over a gait cycle.

This projection for the uncompensated joint power does not include mechanical power dissipation, which is small but nonzero. Therefore, these represent conservative predictions for power consumption without support elements, used only for postprocessing comparisons, not for design.

This method of comparison assumes that the desired joint torques are approximately achieved, in the presence of the support elements. Prior results with the same drivetrain on STEPPR found torque tracking typically within 1%. Furthermore, when torque tracking error exceeded ∼1%, STEPPR fell quickly. Thus, WANDERER's consistent, steady walking itself indicates high-quality torque tracking. For the joints without support elements, power consumption was assumed to be unaffected by the presence of compensations at other joints.

All of the three compensation designs save considerable energy and result in a projected reduction of 235 W or a 43% savings in total actuation power (the joint by joint breakdown is plotted as "FW" in Fig. 6). This compares favorably to the 49% savings predicted by the design analysis, and the joint-by-joint savings are reasonably close to the predictions as well. The plots in Fig. 5 show time series data for each

joint pair utilizing a SE. Each plot shows the mean ± standard deviation joint power over a gait cycle (toe-off to toe-off) using the data from the short laboratory experiment. The typically small standard deviation of power (shown by the shaded areas) illustrates the stepping consistency and the broad benefit of the SEs. The hip spring provides strong benefits during stance. The knee SE has similar behavior, although it modestly costs energy in a region around 65% of the gait cycle. Lastly, the ankle springs provide clear benefit during stance, but cost substantial energy during swing. This is because our current gait keeps the foot parallel to the ground at all times, causing the motors to fight the springs during portions of swing. As gaits mature toward more efficient, humanlike gaits that feature heel-strike and toe-off (potentially requiring a change to foot shape), we expect greater benefits at the ankle [20]. Nonetheless, the ankle springs provide a significant 26% projected motor power savings with the current gait.

C. Efficient Versatile Mobility

A key goal of WANDERER was to achieve low power consumption for behaviors beyond forward walking. The ability to perform a variety of motions with low power consumption is essential to performing diverse missions that involve evaluating the environment (standing), changing direction frequently (turning/sidestepping), or operating in constrained areas (crouched or backward walking). WANDERER is capable of diverse motions and uses its support elements to save energy in these motions. Previous studies of humanoid robots have not examined the energetics of versatile motions. Therefore, the experimental results highlighted below represent a core contribution of this article.

The SEs for WANDERER were designed using data-driven techniques to provide broad energetic benefits with minimal adjustment. We examined the versatility of the SEs by demonstrating a variety of relevant motions which include forward walking (FW), sidestepping (SS), turning (Turn), backward walking (BW), more upright walking (UW), more crouched walking (CW), and standing (Stand). This versatile behavior is highlighted in the accompanying video and illustrates WANDERER's broad walking capability.

The energetic ramifications of the SEs are determined by comparing the uncompensated power and compensated power in the same manner as in the previous section. These savings range from 20% (more crouched walking) to 80% (standing), when power is totaled across all joints. The standing results are particularly interesting and relevant because robots must frequently remain stationary while evaluating or manipulating the environment. Because its drivetrain is fully backdrivable, WANDERER cannot maintain a standing pose without motor torque. Therefore, the actuator power to simply stand in place is projected to be 157 W. The SEs reduce this to a mere 30 W. These benefits were achieved without adjustment to the mechanisms. Larger energy savings are possible with SEs that can switch or self-adjust [21].

The projected energetic savings from each SE design are shown in Fig. 6, which illustrates how the energy savings vary with gait behavior. For example, the benefits from the knee linkage are reduced during highly crouched walking (CW). Nonetheless, energy is saved for all the motions examined. The Hip X spring provides large savings over all walking motions. The projected energy savings from the Hip X spring reach as high as 87%. This benefit substantially exceeds the results seen in our prior work with STEPPR. The ankle spring performance varies with the robot behavior. The ankle springs save up to 98% of power during standing and also provide large benefits during sidestepping and turning. However, very deep crouches cause the robot to fight the springs, costing net energy. Still, this loss is modest, particularly compared to the total SE energy saving projections.

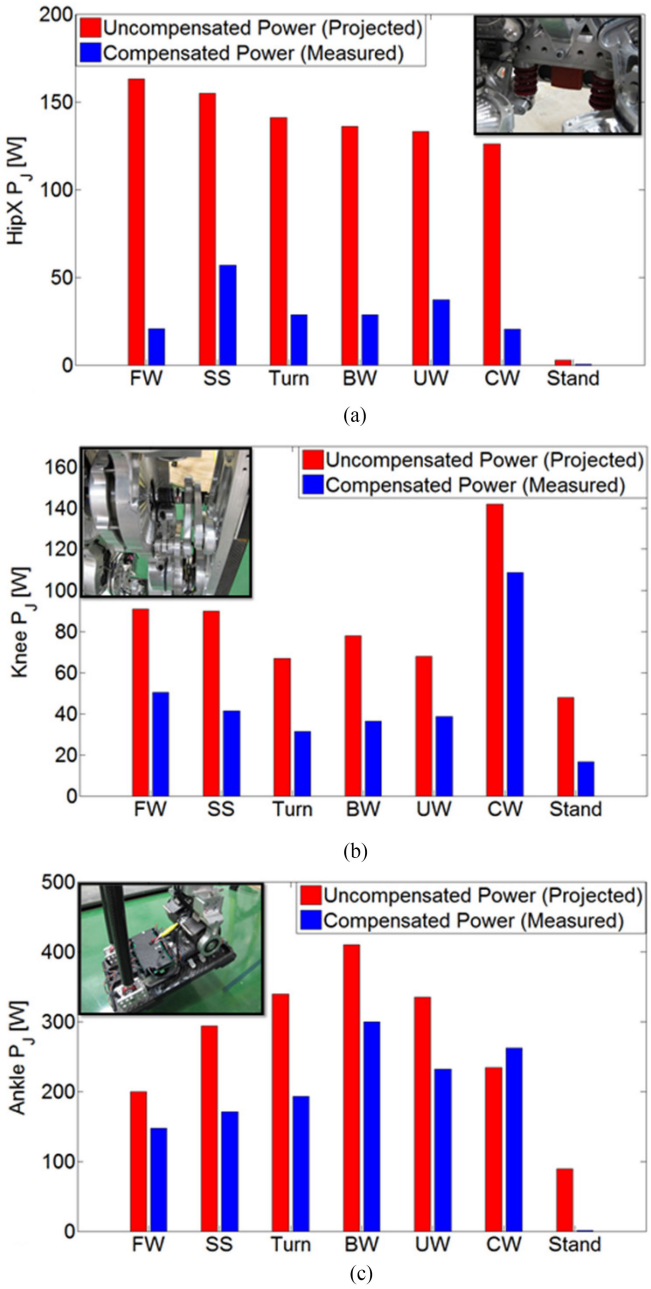

Fig. 6. Power consequences of (a) Hip X spring, (b) Four-bar mechanism at the knee, and (c) Ankle Y spring for a variety of behaviors.

IV. Conclusion

In this article, we presented a novel set of experimental results that illustrated versatile energy efficiency and high endurance. These results demonstrated improved efficiency over our previous works by: first, utilizing large motors operating in efficient regions, second, minimizing gear reductions, and therefore eliminating the need to actively compensate for drivetrain inertia, and third, implementing novel, integrated, and stiff mechanisms to minimize peak torque.

Due to the lack of friction, I^2R losses dominate system inefficiencies. With no need to actively compensate for drivetrain inertia (or friction), e.g., via torque feedback, the motor torques (which are proportional to current, and thus heavily influence I^2R losses) are limited to those

required to produce joint output. Passively shaping the transmission dynamics with support elements further reduced peak motor currents and I^2R losses.

A comparison with our previous prototype, STEPPR, provides a clear illustration of the core contributions of this article. When walking at 0.2 m/s, STEPPR consumed 1000 W for its actuators without support elements. Even with support elements, STEPPR achieved a best COT of 4.4. The motor scaling, reduced hip spacing, and enhanced support elements described in this article enabled WANDERER to consume 310 W at 0.2 m/s, resulting in a COT of 1.73. Comparisons with other robots is challenging because the current literature has not focused on endurance and versatile behaviors.

A primary path to further improve endurance and COT is to improve the robot gait. With the present control paradigm, WANDERER walks most reliably around 0.2 m/s. At this slow speed, quasi-static loads dominate, and dynamic loads are modest. Since COT is proportional to the ratio of power to speed, faster walking is expected to decrease COT and increase walking range. While enhanced walking control remains an area of active research, WANDERER would remain well within its torque and power limits if walking several times faster than its current typical rate. Furthermore, since the set of design gaits used to develop WANDERER's SEs included substantially faster and more dynamic gaits (e.g., human walking at $\sim$1.0 m/s), energy efficiency is expected to persist at higher speeds.

ACKNOWLEDGMENT

The authors would like to acknowledge Nadia Coleman, Dennis Wilder, Timothy Blada, and the late Gregory Brunson. This article describes objective technical results and analysis. Any subjective views or opinions that might be expressed in this article do not necessarily represent the views of the U.S. Department of Energy or the U.S. Government.

REFERENCES

[1] S. Collins *et al.*, "Efficient bipedal robots based on passive-dynamic walkers," *Science*, vol. 307, no 5712, pp. 1082–1085, 2005.
[2] E. Ackerman and E. Guizzo, "The next generation of Boston dynamics' ATLAS robot is quiet, robust, and tether free," IEEE Spectrum, New York, NY, USA, Feb. 2016. [Online]. Available: https://spectrum.ieee.org/automaton/robotics/humanoids/next-generation-of-boston-dynamics-atlas-robot
[3] T. Yang *et al.*, "Design and control of a planar bipedal robot ERNIE with parallel knee compliance," *Auton. Robot*, vol. 25, pp. 317–330, 2008.
[4] N. Radford *et al.*, "Valkyrie: NASA's first bipedal humanoid robot," *J. Field Robot.*, vol. 32, no. 3. 397–419, 2015.
[5] S. Yi *et al.*, "Team THOR's entry in the DARPA robotics challenge trial 2013," *J. Field Robot.*, vol. 32, no. 3, pp. 315–335, 2015.
[6] I. Woo *et al.*, "Mechanical design of the humanoid robot platform, HUBO," *Adv. Robot.*, vol. 21, no. 11, pp. 1305–1322, 2012.
[7] D. Lahr *et al.*, "Early developments of a parallely actuated humanoid, SAFFiR," in *Proc. ASME Mech. Robot. Conf.*, Aug. 2013, pp. 1–7.
[8] S. Seok *et al.*, "Design principles for energy-efficient legged locomotion and implementation on the MIT cheetah robot," *IEEE/ASME Trans. Mech.*, vol. 20, no. 3, 1117–1129, Jun. 2015.
[9] H. Park *et al.*, "High-speed bounding with the MIT Cheetah 2: Control design and experiments," *Int. J. Robot. Res.*, vol. 36, no. 2, pp. 167–192, 2017.
[10] C. Hubicki *et al.*, "ATRIAS: Design and validation of a tether-free 3D-capable spring-mass bipedal robot," *Int. J. Robot. Res.*, vol. 35, no. 12, pp. 1497–1521, 2016.
[11] J. Reher *et al.*, "Realizing dynamic and efficient bipedal locomotion on the humanoid robot DURUS," in *Proc. IEEE Int. Conf. Rob. Automat.*, May 2016, pp. 1794–1801.
[12] S. Buerger *et al.*, "Energy implications of torque feedback control and series elastic actuators for mobile robots," in *Proc. ASME Dyn. Syst. Control Conf.*, Oct. 2018, Paper no. DSCC2018-9141.
[13] A. Mazumdar *et al.*, "Synthetic fiber capstan drives for highly efficient, torque controlled, robotic applications," *IEEE Robot. Automat. Lett.*, vol. 2, no. 2, 554–561, Apr. 2017.
[14] A. Mazumdar *et al.*, "Parallel elastic elements improve energy efficiency on the STEPPR bipedal walking robot," *IEEE/ASME Trans. Mech.*, vol. 22, no. 2, pp. 898–908, Apr. 2017.
[15] H. W. Park, K. Sreenath, J. W. Hurst, and J. W. Grizzle, "Identification of a bipedal robot with a compliant drivetrain," *IEEE Control Syst.*, vol. 31, no. 2, 2011, 63–88, Apr. 2011.
[16] N. Paine *et al.*, "Actuator control for the NASA-JSC valkyrie humanoid robot: A decoupled dynamics approach to torque control of series elastic robots," *J. Field Robot.*, vol. 32, no. 3, pp. 378–396, 2015.
[17] A. Mazumdar *et al.*, "Improving robotic actuator torque density and efficiency through enhanced heat transfer," in *Proc. ASME Dyn. Syst. Control Conf.*, Oct. 2016, pp. 1–10.
[18] S. Seok, A. Wang, D. Otten, and S. Kim, "Actuator design for high force proprioceptive control in fast legged locomotion," in *Proc. IEEE/RSJ Int. Conf. Intell. Robots Syst.*, 2012, pp. 1970–1975.
[19] P. M. Wensing, A. Wang, S. Seok, D. Otten, J. Lang and S. Kim, "Proprioceptive actuator design in the MIT cheetah: Impact mitigation and high-bandwidth physical interaction for dynamic legged robots," *IEEE Trans. Robot.*, vol. 33, no. 3, pp. 509–522, Jun. 2017.
[20] A. Shache *et al.*, "On the expression of joint moments during gait," *Gait Posture*, vol. 25, pp. 440–452, 2007.
[21] S. Spencer *et al.*, "Optimization of adjustable drivetrain assistance mechanisms for efficient robotic bipeds," Sandia Nat. Lab., Albuquerque, NM, USA, Tech. Rep. SAND2019-14374, Nov. 2019.
[22] T. Koolen *et al.*, "Design of a momentum-based control framework and application to the humanoid ATLAS," *Int. J. Humanoid Robot.*, vol. 13, no. 1, 1–34, 2016.
[23] J. Pratt *et al.*, "Capturability-based analysis and control of legged locomotion, Part 1: Theory and application to three simple gait models," *Int. J. Robot. Res.*, vol. 31, no. 10, 1117–1133, 2012.
[24] M. Johnson *et al.*, "Team IHMC's lessons learned from the DARPA robotics challenge: Finding data in the rubble," *J. Field Robot.*, vol. 34, no. 2, pp. 241–261, 2017.
[25] M. Chuah and S. Kim, "Enabling force sensing during ground locomotion: A bio-inspired, multi-axis, composite force sensor using discrete pressure mapping," *IEEE Sensor J.*, vol. 14, no. 5, 1693–1703, May 2014.